

Approximate symmetries, insulators, and superconductivity in continuum-model description of twisted WSe₂

Maine Christos,¹ Pietro M. Bonetti,¹ and Mathias S. Scheurer²

¹*Department of Physics, Harvard University, Cambridge MA 02138, USA*

²*Institute for Theoretical Physics III, University of Stuttgart, 70550 Stuttgart, Germany*

Motivated by the recent discovery of superconductivity in twisted bilayer WSe₂, we analyze the correlated physics in this system in the framework of a continuum model for the moiré superlattice. Using the symmetries in a fine-tuned limit of the system, we identify the strong-coupling ground states and their fate when the perturbations caused by finite bandwidth, displacement field, and the phase of the intralayer potential are taken into account. We classify the superconducting instabilities and, employing a spin-fermion-like model, study the superconducting instabilities in proximity to these insulating particle-hole orders. This reveals that only a neighboring intervalley coherent phase (with zero or finite wave vector) is naturally consistent with the observed superconducting state. Depending on details, the superconductor will be nodal or a chiral gapped state while further including electron-phonon coupling leads to a fully gapped, time-reversal symmetric pairing state.

The observation of superconductivity in twisted bilayer graphene [1] has sparked enormous interest, ultimately making the field of twisted van der Waals moiré superlattices one of the most active areas of current condensed matter research [2, 3]. While tight-binding model descriptions on the moiré scale have been discussed and developed early on [4–6], the continuum model [7–10], supplemented by interactions, has remained the central model studied by theorists; important insights and guidance have been provided by unrestricted mean-field and analytical strong-coupling studies [11–19] of continuum models. Recent experiments [20–26] on twisted graphene systems yield crucial constraints for superconductivity and point towards an interesting pairing state and mechanism, the nature of which is still under debate [27–34].

On top of previous reports of insulating behavior and symmetry breaking in twisted bilayer WSe₂ [35–37] as well as indications of superconductivity [35], very recently, a genuine superconducting phase was observed [38, 39]. Most remarkably, the superconducting state appears close to the point where the insulator is suppressed, hinting at an electronic pairing mechanism. While there have been multiple insightful theoretical studies [40–53] of the moiré Hubbard model of twisted bilayer WSe₂ [54], of extensions thereof, as well as of its strong-coupling spin models, and of patch models [52, 55], we here complement these works by studying the correlated physics directly in a continuum description of the moiré superlattice. We perform a strong-coupling analysis for the insulators, classify the possible superconducting phases and study the resulting pairing states stabilized by fluctuations of the neighboring insulators. Our primary focus is on the symmetries and energetics of these phases and not on the possibility of a direct transition between the two, which could be explained by a spin liquid [56]. We hope that our work can help elucidate the interplay of insulating and superconducting physics in the continuum model of twisted bilayer WSe₂, which combined with future ex-

periments, could also help resolve related open questions in graphene-based moiré systems.

Model and symmetries.—For the non-interacting physics, we start from the continuum model [41, 42, 54] $H_c = \int_{\mathbf{r}} \sum_{\eta=\pm} \sum_{\ell,\ell'=\pm} c_{\eta,\ell}^\dagger(\mathbf{r}) h_{\ell,\ell'}^\eta(\nabla, \mathbf{r}) c_{\eta,\ell'}(\mathbf{r})$ where

$$h^+ = -\frac{(-i\nabla - \ell_z \boldsymbol{\kappa})^2}{2m} + \frac{D}{2} \ell_z + 2V \sum_{j=1,3,5} \cos(\mathbf{g}_j \mathbf{r} + \ell_z \psi) + [\ell_+ w (1 + e^{-i\mathbf{g}_2 \mathbf{r}} + e^{-i\mathbf{g}_3 \mathbf{r}}) / 2 + \text{H.c.}] \quad (1)$$

describes the states in valley K (spin- \uparrow). In Eq. (1), D is the displacement field, ℓ_j are Pauli matrices in layer space, $\ell_+ = \ell_x + i\ell_y$, $\mathbf{g}_j = R(\pi(j-1)/3)\mathbf{g}_1$, with $R(\varphi)$ rotating 2D vectors by φ , $\mathbf{g}_{1,2}$ are the basis vectors of the reciprocal lattice (RL) on the moiré scale, and $\boldsymbol{\kappa}$ is the K-point in the single layer Brillouin zone. The Hamiltonian in the other valley (spin- \downarrow) is just related by time-reversal symmetry, $h_{\ell,\ell'}^- = (h_{\ell,\ell'}^+)^*$.

Apart from three-fold rotational symmetry, C_{3z} , reflection, m_x , along the xz -plane, U(1)-valley symmetry, $U(1)_v : c(\mathbf{r}) \rightarrow e^{i\eta_z \varphi} c(\mathbf{r})$, and time-reversal symmetry $\Theta = i\eta_y \mathcal{K}$ [57], where η_j are Pauli matrices in valley/spin space and \mathcal{K} denotes complex conjugation, the continuum model (1) exhibits the following symmetries: if there is no displacement field, $D = 0$, the Hamiltonian is invariant under the (unitary) “intervalley inversion symmetry” $\mathcal{I} : c(\mathbf{r}) \rightarrow \ell_x c(-\mathbf{r})$. As it will help us understand the correlated physics later on, we will also consider the limit $\psi \in \pi\mathbb{Z}$ yielding the additional “anti-unitary C_{2z} symmetry” \mathcal{C}_2 with action $c(\mathbf{r}) \rightarrow c(-\mathbf{r})$ (and additional complex conjugation).

Since we are interested in the low-energy physics, we will only include the single band per valley that intersects the chemical potential and, thus, leads to Fermi surfaces. Denoting the associated band energies by $E_{\mathbf{k},\eta} = \epsilon_{\mathbf{k}} + \eta \delta \epsilon_{\mathbf{k}}$, Θ implies $\epsilon_{\mathbf{k}} = \epsilon_{-\mathbf{k}}$ and $\delta \epsilon_{\mathbf{k}} = -\delta \epsilon_{-\mathbf{k}}$. Meanwhile \mathcal{C}_2 has no consequences for the band energies (only for the wave functions to be discussed below) and \mathcal{I} , if

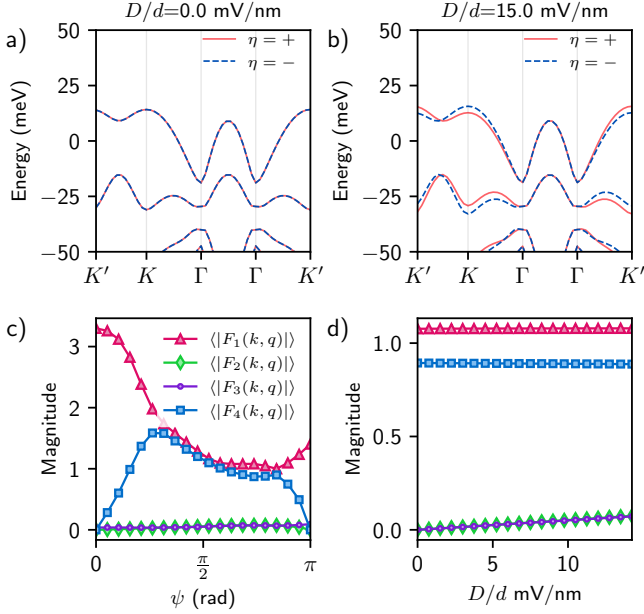


FIG. 1: Band structure of the continuum model in Eq. (1) at (a) $D/d = 0$ mV/nm and (b) $D/d = 15$ mV/nm. We also plot the four components of the form factors in Eq. (2) as a function of (c) ψ for $D/d = 14.25$ mV/nm and (d) as a function of D for $\psi = 128^\circ$. Here $d \simeq 0.26$ e · nm is the dipole-moment relating D to the electric field [38]. All other model parameters are the same as those in [41] unless otherwise specified.

present, enforces $\delta\epsilon_{\mathbf{k}} = 0$, i.e., the band energies will be even in \mathbf{k} and identical in the two valleys. These features are clearly visible in our band calculations shown in Fig. 1(a,b). Denoting the associated electronic annihilation operators in those bands by $d_{\mathbf{k},\eta}$, we summarize all symmetries in Table I.

To include interaction effects, we add the Coulomb interaction, also projected to the two bands at the Fermi level, yielding the total Hamiltonian $H = H_0 + H_1$, where the non-interacting and interacting parts are given by $H_0 = \sum_{\mathbf{k},\eta} E_{\mathbf{k},\eta} d_{\mathbf{k},\eta}^\dagger d_{\mathbf{k},\eta}$ and $H_1 = \frac{1}{2N} \sum_{\mathbf{q}} V(\mathbf{q}) \rho_{\mathbf{q}} \rho_{-\mathbf{q}}$, respectively, with density operator $\rho_{\mathbf{q}} = \sum_{\mathbf{k},\eta} F_{\eta}(\mathbf{k}, \mathbf{q}) d_{\mathbf{k}+\mathbf{q},\eta}^\dagger d_{\mathbf{k},\eta}$. At this point, the precise form of $V(\mathbf{q})$ is not important; we only assume that $V(\mathbf{q}) = V(-\mathbf{q}) \geq 0$ (repulsive). We further already used $U(1)_v$ to constrain the form factors, $F_{\eta}(\mathbf{k}, \mathbf{q})$, to be diagonal in the valley index. Let us expand these form factors using real coefficients F_j ,

$$F_{\eta}(\mathbf{k}, \mathbf{q}) = F_1(\mathbf{k}, \mathbf{q}) + iF_2(\mathbf{k}, \mathbf{q}) + \eta F_3(\mathbf{k}, \mathbf{q}) + i\eta F_4(\mathbf{k}, \mathbf{q}), \quad (2)$$

where Θ implies further

$$F_{1,4}(\mathbf{k}, \mathbf{q}) = F_{1,4}(-\mathbf{k}, -\mathbf{q}), \quad F_{2,3}(\mathbf{k}, \mathbf{q}) = -F_{2,3}(-\mathbf{k}, -\mathbf{q}). \quad (3)$$

TABLE I: Symmetries S (including redundant combinations for clarity, see text for more details), their representation on the operators in the band space, when they are present, and the most relevant consequences for our analysis.

S	unitary	$Sd_{\mathbf{k}}S^{-1}$	Condition	Consequences
$U(1)_v$	✓	$e^{i\varphi\eta z} d_{\mathbf{k}}$	—	$F_{\eta,\eta'} \propto \delta_{\eta,\eta'}$
Θ	✗	$i\eta_y d_{-\mathbf{k}}$	—	$E_{\mathbf{k},\eta} = E_{-\mathbf{k},-\eta}$, Eq. (3)
C_{3z}	✓	$d_{C_{3z}\mathbf{k}}$	—	$E_{\mathbf{k},\eta} = E_{C_{3z}\mathbf{k},\eta}$
m_x	✓	$i\eta_y d_{m_x\mathbf{k}}$	—	$E_{\mathbf{k},\eta} = E_{m_x\mathbf{k},-\eta}$
Θm_x	✗	$-d_{-m_x\mathbf{k}}$	—	$E_{\mathbf{k},\eta} = E_{-m_x\mathbf{k},\eta}$
\mathcal{I}	✓	$d_{-\mathbf{k}}$	$D = 0$	$E_{\mathbf{k},\eta} = E_{-\mathbf{k},\eta}$
$\Theta\mathcal{I}$	✗	$i\eta_y d_{\mathbf{k}}$	$D = 0$	$F_2 = F_3 = 0$
\mathcal{C}_2	✗	$d_{\mathbf{k}}$	$\psi \in \pi\mathbb{Z}$	$F_2 = F_4 = 0$

At $D = 0$, the additional \mathcal{I} symmetry implies that $F_2 = F_3 = 0$. If we further set $\psi \in \pi\mathbb{Z}$, also F_4 has to vanish as a result of \mathcal{C}_2 and we are simply left with $\rho_{\mathbf{q}} = \sum_{\mathbf{k},\eta} F_1(\mathbf{k}, \mathbf{q}) d_{\mathbf{k}+\mathbf{q},\eta}^\dagger d_{\mathbf{k},\eta}$. We have verified these conclusions by diagonalization of the continuum model, as illustrated in Fig. 1(c,d). In combination with \mathcal{I} implying $\delta\epsilon_{\mathbf{k}} = 0$, the Hamiltonian is invariant under an arbitrary, momentum independent $SU(2)$ rotation in valley space, $d_{\mathbf{k}} \rightarrow U d_{\mathbf{k}}$, $U = e^{i\varphi\eta_j}$, for $D = 0$ and $\psi \in \pi\mathbb{Z}$.

Correlated insulators.—To study interacting ground states at half filling, we start from this simple limit and further set the bandwidth W to zero. Consider the family of product states as candidates for $\nu = 1$

$$|\hat{\mathbf{n}}\rangle := \prod_{\mathbf{k}} \left(d_{\mathbf{k}}^\dagger U_{\hat{\mathbf{n}}}^\dagger \right)_+ |0\rangle, \quad U_{\hat{\mathbf{n}}}^\dagger \eta_z U_{\hat{\mathbf{n}}} = \hat{\mathbf{n}} \cdot \boldsymbol{\eta}, \quad (4)$$

where $\hat{\mathbf{n}}$ is a three-component unit vector. Due to the simple form $\rho_{\mathbf{q}} = \sum_{\mathbf{k},\eta} F_1(\mathbf{k}, \mathbf{q}) d_{\mathbf{k}+\mathbf{q},\eta}^\dagger d_{\mathbf{k},\eta}$ of the density operator, we find

$$\rho_{\mathbf{q}} |\hat{\mathbf{n}}\rangle = \sum_{\mathbf{G} \in \text{RL}} \delta_{\mathbf{q},\mathbf{G}} f_{\mathbf{G}} |\hat{\mathbf{n}}\rangle, \quad (5)$$

with $f_{\mathbf{G}} = \sum_{\mathbf{k}} F_1(\mathbf{k}, \mathbf{G})$, i.e., the state is annihilated by the shifted density operator $\bar{\rho}_{\mathbf{q}} := \rho_{\mathbf{q}} - \sum_{\mathbf{G}} \delta_{\mathbf{q},\mathbf{G}} f_{\mathbf{G}}$. Upon writing $H_1 = \bar{H}_1 + \Delta H_1$ with $\bar{H}_1 = \frac{1}{2N} \sum_{\mathbf{q}} V(\mathbf{q}) \bar{\rho}_{\mathbf{q}}^\dagger \bar{\rho}_{\mathbf{q}}$ and $\Delta H_1 = \sum_{\mathbf{G}} V(\mathbf{G}) f_{\mathbf{G}} (2\rho_{-\mathbf{G}} - f_{-\mathbf{G}})$. If we further assume the “flat-metric condition” [58], i.e., that $F_1(\mathbf{k}, \mathbf{G})$ is independent of \mathbf{k} , which we verified holds approximately for the model (1) [59], we get that $\rho_{\mathbf{G}}$ is proportional to the particle-number operator; in that case, ΔH_1 is just a constant at fixed filling. Since $\bar{H}_1 |\hat{\mathbf{n}}\rangle = 0$ by virtue of Eq. (5) and noting that \bar{H}_1 is positive semi-definite, we conclude that any $|\hat{\mathbf{n}}\rangle$ in Eq. (4) is an exact ground state of the interacting part of the Hamiltonian.

When also including the dispersion part of the Hamiltonian H_0 , these states still remain exact, degenerate eigenstates of the full Hamiltonian for $D = 0$ and $\psi \in \pi\mathbb{Z}$.

Note, however, that they will cease to be the ground state above a certain value of the bandwidth. While eventually, the system is expected to become a symmetry unbroken metal at large bandwidth, there might also be an intermediate regime where translational symmetry breaking order develops, as seen in triangular lattice Hubbard models [41–45, 49–51, 60–63].

Dispersion as perturbation.—We next analyze what happens when the SU(2) symmetry is broken due to finite $\delta\epsilon_{\mathbf{k}}$ in the dispersion, i.e., when D is turned on. It is straightforward to see that, within first order perturbation theory, there is no energetic splitting between the states in Eq. (4), which is a consequence of $\sum_{\mathbf{k}} \delta\epsilon_{\mathbf{k}} = 0$ (imposed by Θ). Since η_z ($\eta_{x,y}$) commutes (anti-commute) with the associated perturbation $\eta_z\delta\epsilon_{\mathbf{k}}$, its second order contributions is still zero (finite) [18]; this can also be directly seen by noting that $|\hat{e}_z\rangle$ is still an exact eigenstate of the full Hamiltonian while $|\hat{e}_{x,y}\rangle$ are not. Since corrections to the ground state energy in second order of perturbation theory are always non-positive, this shows that the intervalley coherent (IVC) states $|\hat{e}_{x,y}\rangle$ are energetically favored over the valley polarized (VP) state $|\hat{e}_z\rangle$. As such, superexchange processes controlled by D break the SU(2) symmetry in a way that leads to an “easy plane” for $\hat{\mathbf{n}}$.

Form factors as perturbation.—Another important perturbation to the SU(2) manifold comes from the form factors. As discussed above, turning on D at $\psi \in \pi\mathbb{Z}$ allows for finite F_3 in Eq. (2), while $\psi \notin \pi\mathbb{Z}$ at $D = 0$ admixes F_4 to the F_1 component. Finally, when both $\psi \notin \pi\mathbb{Z}$ and $D \neq 0$ also F_2 can become finite. To analyze which state is favored by these perturbations, we compute the change $\Delta E(\hat{\mathbf{n}})$ of $\langle \hat{\mathbf{n}} | H_1 | \hat{\mathbf{n}} \rangle$ associated with the form factors $F_{j>1}$; using $F_j(\mathbf{k}, \mathbf{G}) = s_j F_j(-\mathbf{k}, \mathbf{G})$ with $s_{1,2} = -s_{3,4} = 1$, as follows from Θ and Hermiticity, we obtain

$$\Delta E(\hat{\mathbf{n}}) = \Delta E_0 - \sum_{\mathbf{k}, \mathbf{q}} \frac{V(\mathbf{q})}{2N} [F_3^2(\mathbf{k}, \mathbf{q}) + F_4^2(\mathbf{k}, \mathbf{q})] \hat{n}_z^2, \quad (6)$$

where ΔE_0 is an SU(2)-invariant and, thus, $\hat{\mathbf{n}}$ -independent contribution. Therefore, both the ψ - and D -induced corrections to the form factors lead to an “easy axis” for $\hat{\mathbf{n}}$, favoring the VP state. This also holds beyond this simple variational calculation (if the flat-metric condition holds) by noting that Eq. (5) still applies for $|\pm\hat{e}_z\rangle$ (albeit with a modified $f_{\mathbf{G}} = \sum_{\mathbf{k}} [F_1(\mathbf{k}, \mathbf{G}) + iF_2(\mathbf{k}, \mathbf{G})]$), but not for $|\pm\hat{e}_{x,y}\rangle$, establishing VP as the ground state when $\psi \notin \pi\mathbb{Z}$ and/or $D \neq 0$ in the flat-band limit.

Taken together, depending on whether the D -induced SU(2)-symmetry breaking in the band structure or the additional form factors induced by D and ψ are larger, we get an IVC or VP ground state. At $D = 0$, the VP ground state is favored for generic values of ψ . As indicated by experiment, additional corrections to this description, e.g., coming from thermal fluctuations in the

TABLE II: Possible pairing states classified according to the IRs of the point group C_{3v} of the continuum model. We list the minimal number of nodes on a Fermi surface encircling the Γ point with the three values referring to first $D \neq 0$ (and sufficiently large, see text), second $D = 0$ and \mathcal{I} even, and, third, $D = 0$ and \mathcal{I} odd, respectively. As a result of Θ in the normal state, all basis functions are real.

Furthermore, $\chi_{\mathbf{k}}$ and $(X_{\mathbf{k}}, Y_{\mathbf{k}})$ transform as a scalar and vector under C_{3v} , respectively, and $X_{\mathbf{k}} = X_{-m_x\mathbf{k}}$, $Y_{\mathbf{k}} = -Y_{-m_x\mathbf{k}}$. In the last column, we list the additional two possible pairing states associated with \mathcal{I} at $D = 0$.

IR of C_{3v}	form of $\Delta_{\mathbf{k}}$	nodes	for $D = 0$
A_1	$\chi_{\mathbf{k}} = \chi_{-m_x\mathbf{k}}$	0/0/6	$\chi_{\mathbf{k}} = \pm\chi_{-\mathbf{k}} = \pm\chi_{m_x\mathbf{k}}$
A_2	$\chi_{\mathbf{k}} = -\chi_{-m_x\mathbf{k}}$	6/12/6	$\chi_{\mathbf{k}} = \pm\chi_{-\mathbf{k}} = \mp\chi_{m_x\mathbf{k}}$
$E(1, 0)$	$X_{\mathbf{k}}$	2/4/2	$X_{\mathbf{k}} = \pm X_{-\mathbf{k}} = \pm X_{m_x\mathbf{k}}$
$E(0, 1)$	$Y_{\mathbf{k}}$	2/4/2	$X_{\mathbf{k}} = \pm Y_{-\mathbf{k}} = \mp Y_{m_x\mathbf{k}}$
$E(1, i)$	$X_{\mathbf{k}} + iY_{\mathbf{k}}$	0/0/0	

vicinity of the SU(2) symmetric point, the finite bandwidth and additional corrections to the interaction, the system ceases to be an interaction-induced insulator and, instead, develops superconductivity for small D .

Classification of pairing.—Before we study the energetics of superconductivity, we use the symmetries in Table I to classify the different forms of pairing instabilities. As a result of $U(1)_v$, pairing is either entirely intra- or intervalley and we focus on the latter here as there are no indications [38, 39] that the normal state above T_c has broken time-reversal symmetry. On the mean-field level, the superconducting order parameter couples as $H_{\text{MF}} = \sum_{\mathbf{k}, \eta} d_{\mathbf{k}, \eta}^\dagger \Delta_{\mathbf{k}, \eta} d_{-\mathbf{k}, -\eta}^\dagger$ to the low-energy electrons. Fermi-Dirac statistics implies $\Delta_{\mathbf{k}, \eta} = -\Delta_{-\mathbf{k}, -\eta}$ such that we will focus on $\Delta_{\mathbf{k}} := \Delta_{\mathbf{k}, +}$ in the following without loss of generality.

Using the irreducible representations (IRs) of the point group C_{3v} , we find five different pairing instabilities, as summarized in Table II—two associated with the one-dimensional IRs, A_1 , A_2 , and three for the two-dimensional IR E . We emphasize that, by virtue of the intervalley nature of m_x , its action on the superconducting order parameter reads as $\Delta_{\mathbf{k}} \rightarrow \Delta_{-m_x\mathbf{k}}$. Importantly, at $D = 0$, the additional intravalley inversion symmetry \mathcal{I} leads to a splitting of each of the above-mentioned IRs $g \in \{A_1, A_2, E\}$ into two, which we denote by g^\pm and are associated with the two possible signs \pm in the constraint $\Delta_{\mathbf{k}} = \pm\Delta_{-\mathbf{k}}$. This is indicated in the last column of Table II. Depending on the sign, \mathcal{I} does or does not give rise to additional symmetry-protected nodes. By continuity, these additional nodes are stable against finite D .

Energetics of superconductivity.—As in both experiments [38, 39] the superconducting state appears in close proximity to the insulating phase, we first assume that fluctuations of the latter provide the pairing glue. There-

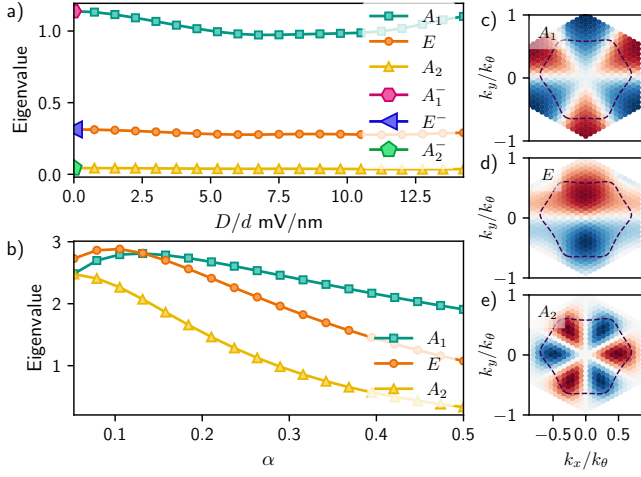


FIG. 2: Largest eigenvalues of the LGE as a function of (a) displacement field D and (b) the mass parameter α of the fluctuating bosons corresponding to the IRs A_1 (A_1^-), A_2 (A_2^-), and E (E^-) for $D > 0$ ($D = 0$). The order parameter $\Delta_{\mathbf{k}}$ of the leading, subleading, and third leading states in (a) at $D/d = 14.25$ mV/nm are shown in (c), (d), and (e) respectively.

fore, we study, in analogy to the celebrated spin-fermion model [64] for the high-temperature superconductors, an effective model, where the low-energy fermions $d_{\mathbf{k}}$ are coupled to collective bosons $\phi_j(\mathbf{q}) = \phi_j^\dagger(-\mathbf{q})$ via

$$H_{\text{fb}} = \sum_{\mathbf{k}, \mathbf{q}} \sum_{j=x,y,z} d_{\mathbf{k}+\mathbf{q}}^\dagger \lambda_j(\mathbf{k}, \mathbf{q}) d_{\mathbf{k}} \phi_j(\mathbf{q}). \quad (7)$$

Here $j = x, y$ describe IVC and $j = z$ valley fluctuations constraining their associated form factors $\lambda_{x,y}$ and λ_z to be valley off-diagonal and diagonal, respectively, while time-reversal implies $\eta_y \lambda_j^*(\mathbf{k}, \mathbf{q}) \eta_y = -\lambda_j(-\mathbf{k}, -\mathbf{q})$.

Inspired by the strong-coupling analysis above, we start by assuming that the (static) susceptibility $\chi(\mathbf{q})$ of the collective bosons is peaked at $\mathbf{q} = 0$. The boson ϕ_z will mediate a repulsive intra-valley Cooper channel interaction and is, thus, not expected to stabilize superconductivity. To demonstrate that, we solve the linearized gap equations (LGE) numerically, using $\chi(\mathbf{q}) = C \frac{\alpha}{\alpha^2 + \mathbf{q}^2/k_g^2}$ and taking λ_j in Eq. (7) to be the projections of η_j onto the Bloch states of the band at the Fermi level [59]; here α parametrizes the bosonic mass which becomes smaller when approaching the neighboring insulating phase and we take $\alpha = 1$ and $C/A_{\text{moire}} = 1.7$ meV unless otherwise specified. Indeed, we find vanishingly small eigenvalues for the case of fluctuations of ϕ_z . This is to be contrasted with fluctuations of $\phi_{x,y}$, which mediate an attractive intervalley interaction, in the sense that they favor $\Delta_{\mathbf{k},\eta} \simeq \Delta_{\mathbf{k},-\eta}$. However, due to the Fermi-Dirac constraint $\Delta_{\mathbf{k},\eta} = -\Delta_{-\mathbf{k},-\eta}$ and the significantly larger band separation compared to twisted bi- and tri-layer graphene, where interband pairing is stabilized by

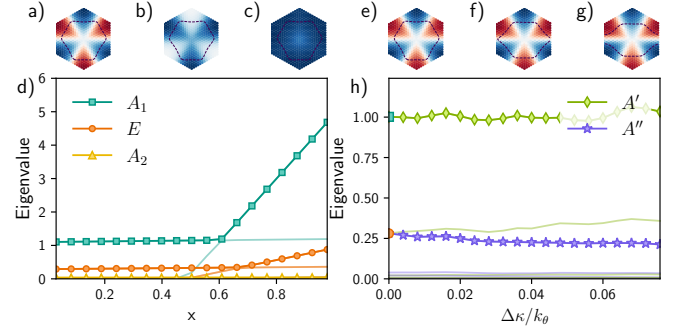


FIG. 3: Tuning the relative strength of the pairing interactions from purely IVC fluctuations ($x = 0$) to only electron-phonon coupling ($x = 1$), we show $\Delta_{\mathbf{k}}$ of the leading state for (a) $x = 0$, (b) $x = 0.61$, (c) $x = 1$, and the evolution of the eigenvalues of the LGE in at $D/d = 14.25$ mV/nm (d); here lines with the same color correspond to the same IR of C_{3v} . (e-h) show the same quantities but as a function of $\Delta\kappa$, capturing the C_{3z} breaking due to strain or nematic order, and using the IRs of C_s at $D/d = 5$ mV/nm. The plot markers at $\Delta\kappa = 0$ refer to the legend in (d).

these types of interactions [32], we here have $\Delta_{\mathbf{k}} \simeq -\Delta_{-\mathbf{k}}$ and, thus, sign changes of the order parameter in the Brillouin zone. While this indicates that the order parameter transforms under an \mathcal{I} -odd representation for $D \rightarrow 0$, all of A_1^- , A_2^- , and E^- are in principle possible and the outcome depends on energetics. In line with these considerations, we find in our numerics in Fig. 2(a,b) that the states with largest pairing strength (eigenvalue) not only emanate from \mathcal{I} -odd IRs [see (a)] but also stay approximately odd in \mathbf{k} in the experimentally relevant range of D , see Fig. 2(c-e). We further observe that the A_1^- and E^- states are competing and which of the two is favored depends on the proximity to the insulator (the value of α). As a result of the additional symmetry-imposed lines of zeros of $\Delta_{\mathbf{k}}$ at the zone boundary, the A_2^- state in Fig. 2(e) has very small eigenvalues.

As noted above, the significant value of the dispersion can lead to ordering at finite wave vector; this is why we also considered $\chi(\mathbf{q})$ that are peaked at three, C_{3z} related, minima $(C_{3z})^{j-1} \mathbf{q}_f$ with \mathbf{q}_f being varied from $\mathbf{q}_f = 0$ to the K point. We find [59] that the above conclusions about the order of eigenvalues is not affected until \mathbf{q}_f gets close to the K point, where A_2 can become the leading state; its eigenvalue is, however, comparatively small.

Motivated by indications that the electron-phonon coupling in monolayer transition metal dichalcogenides can become sizable [65], we here study the additional impact of phonons on pairing, focusing on A_1' optical phonons of the constituent monolayers [66], seen in Raman studies [65, 67]. These can mediate an attractive intravalley interaction [59] and are, thus, expected to favor the conventional A_1^+ state. This can also be seen

in our numerics in Fig. 3(a-d), where we find a transition (crossover at $D \neq 0$) from (primarily) A_1^- to A_1^+ , when phonon-mediated interactions become comparable to those induced by IVC fluctuations. We here introduced the dimensionless parameter $x \in [0, 1]$ parameterizing the ratio $x/(1-x)$ of electron-phonon- to IVC-fluctuation-induced interactions [59].

We finally discuss the impact of rotational symmetry breaking, as it can result from strain [68, 69] or possibly electronic nematic order. We capture this symmetry reduction by the shift of magnitude $\Delta\kappa$ of κ in Eq. (1); choosing for concreteness a high symmetry direction of this shift that retains the reflection symmetry m_x , the point group (at finite D) becomes C_s . We can see in Fig. 3(e-g) that the states associated with IR E split into two—one even (IR A' of C_s) and one odd (A'') under m_x . While the leading state continues to be the previous A_1 state (now A'), we observe that strain can, for very large values, reduce the number of nodal points [see (g)].

Conclusion.—In summary, we have studied the possible insulating phases as a result of Coulomb interaction in a continuum-model description of twisted WSe₂, showing that IVC or VP is favored depending on whether the D -induced SU(2)-breaking perturbations in the bandwidth or in the form factors dominate. Using the valley-fermion model description of the pairing glue in Eq. (7), we find that only IVC fluctuations are consistent with superconductivity, necessarily leading to a superconducting order

parameter with nodes or broken time-reversal symmetry. As samples with superconductivity show insulating (superconducting) behavior at larger D (smaller D), this IVC-based pairing glue is also consistent with the strong-coupling analysis. The superconductor becomes fully gapped when additional interactions from phonons are significant. There are many natural directions for future works, such as including more bands and generalizing this continuum-model study to heterobilayers [70–72] or more exotic novel forms of moiré superlattices [73, 74].

Note added.—Just before posting our work, Ref. 75 appeared online, which also discusses pairing in twisted twisted WSe₂ in the continuum model.

ACKNOWLEDGMENTS

M.S.S. acknowledge funding by the European Union (ERC-2021-STG, Project 101040651—SuperCorr). Views and opinions expressed are however those of the authors only and do not necessarily reflect those of the European Union or the European Research Council Executive Agency. Neither the European Union nor the granting authority can be held responsible for them. M.C. and P.M.B. acknowledge funding from U.S. National Science Foundation grant No. DMR-2245246. M.C. thanks Ming Xie for helpful conversations on pairing mechanisms.

-
- [1] Y. Cao, V. Fatemi, S. Fang, K. Watanabe, T. Taniguchi, E. Kaxiras, and P. Jarillo-Herrero, “Unconventional superconductivity in magic-angle graphene superlattices,” *Nature* **556**, 43 (2018).
 - [2] E. Y. Andrei and A. H. MacDonald, “Graphene bilayers with a twist,” *Nature Materials* **19**, 1265 (2020).
 - [3] L. Balents, C. R. Dean, D. K. Efetov, and A. F. Young, “Superconductivity and strong correlations in moiré flat bands,” *Nature Physics* **16**, 725 (2020).
 - [4] J. Kang and O. Vafek, “Symmetry, maximally localized wannier states, and a low-energy model for twisted bilayer graphene narrow bands,” *Phys. Rev. X* **8**, 031088 (2018).
 - [5] M. Koshino, N. F. Q. Yuan, T. Koretsune, M. Ochi, K. Kuroki, and L. Fu, “Maximally localized wannier orbitals and the extended hubbard model for twisted bilayer graphene,” *Phys. Rev. X* **8**, 031087 (2018).
 - [6] H. C. Po, L. Zou, T. Senthil, and A. Vishwanath, “Faithful tight-binding models and fragile topology of magic-angle bilayer graphene,” *Phys. Rev. B* **99**, 195455 (2019).
 - [7] J. M. B. L. Dos Santos, N. M. R. Peres, and A. H. C. Neto, “Graphene bilayer with a twist: electronic structure,” *Phys. Rev. Lett.* **99**, 256802 (2007).
 - [8] E. J. Mele, “Commensuration and interlayer coherence in twisted bilayer graphene,” *Phys. Rev. B* **81**, 161405 (2010).
 - [9] R. Bistritzer and A. H. MacDonald, “Moiré bands in twisted double-layer graphene,” *Proc. Natl. Acad. Sci. U.S.A.* **108**, 12233 (2011).
 - [10] J. M. B. L. Dos Santos, N. M. R. Peres, and A. H. C. Neto, “Continuum model of the twisted graphene bilayer,” *Phys. Rev. B* **86**, 155449 (2012).
 - [11] N. Bultinck, E. Khalaf, S. Liu, S. Chatterjee, A. Vishwanath, and M. P. Zaletel, “Ground state and hidden symmetry of magic-angle graphene at even integer filling,” *Phys. Rev. X* **10**, 031034 (2020).
 - [12] M. Xie and A. H. MacDonald, “Nature of the correlated insulator states in twisted bilayer graphene,” *Phys. Rev. Lett.* **124**, 097601 (2020).
 - [13] Y. Zhang, K. Jiang, Z. Wang, and F. Zhang, “Correlated insulating phases of twisted bilayer graphene at commensurate filling fractions: A hartree-fock study,” *Phys. Rev. B* **102**, 035136 (2020).
 - [14] F. Xie, N. Regnault, D. Călugăru, B. A. Bernevig, and B. Lian, “Twisted symmetric trilayer graphene. ii. projected hartree-fock study,” *Phys. Rev. B* **104**, 115167 (2021).
 - [15] S. Liu, E. Khalaf, J. Y. Lee, and A. Vishwanath, “Nematic topological semimetal and insulator in magic-angle bilayer graphene at charge neutrality,” *Phys. Rev. Res.* **3**, 013033 (2021).
 - [16] B. Lian, Z.-D. Song, N. Regnault, D. K. Efetov, A. Yaz

- dani, and B. A. Bernevig, “Twisted bilayer graphene. iv. exact insulator ground states and phase diagram,” *Phys. Rev. B* **103**, 205414 (2021).
- [17] Y. H. Kwan, G. Wagner, T. Soejima, M. P. Zaletel, S. H. Simon, S. A. Parameswaran, and N. Bultinck, “Kekulé spiral order at all nonzero integer fillings in twisted bilayer graphene,” *Phys. Rev. X* **11**, 041063 (2021).
- [18] M. Christos, S. Sachdev, and M. S. Scheurer, “Correlated insulators, semimetals, and superconductivity in twisted trilayer graphene,” *Phys. Rev. X* **12**, 021018 (2022).
- [19] G. Wagner, Y. H. Kwan, N. Bultinck, S. H. Simon, and S. A. Parameswaran, “Global phase diagram of the normal state of twisted bilayer graphene,” *Phys. Rev. Lett.* **128**, 156401 (2022).
- [20] M. Oh, K. P. Nuckolls, D. Wong, R. L. Lee, X. Liu, K. Watanabe, T. Taniguchi, and A. Yazdani, “Evidence for unconventional superconductivity in twisted bilayer graphene,” *Nature* **600**, 240 (2021).
- [21] H. Kim, Y. Choi, C. Lewandowski, A. Thomson, Y. Zhang, R. Polski, K. Watanabe, T. Taniguchi, J. Alicea, and S. Nadj-Perge, “Evidence for unconventional superconductivity in twisted trilayer graphene,” *Nature* **606**, 494 (2022).
- [22] X. Liu, N. J. Zhang, K. Watanabe, T. Taniguchi, and J. I. A. Li, “Isospin order in superconducting magic-angle twisted trilayer graphene,” *Nature Physics* **18**, 522 (2022).
- [23] J.-X. Lin, P. Siriviboon, H. D. Scammell, S. Liu, D. Rhodes, K. Watanabe, T. Taniguchi, J. Hone, M. S. Scheurer, and J. I. A. Li, “Zero-field superconducting diode effect in small-twist-angle trilayer graphene,” *Nature Physics* **18**, 1221 (2022).
- [24] C. Chen, K. P. Nuckolls, S. Ding, W. Miao, D. Wong, M. Oh, R. L. Lee, S. He, C. Peng, D. Pei, Y. Li, S. Zhang, J. Liu, Z. Liu, C. Jozwiak, A. Bostwick, E. Rotenberg, C. Li, X. Han, D. Pan, X. Dai, C. Liu, B. A. Bernevig, Y. Wang, A. Yazdani, and Y. Chen, “Strong inter-valley electron-phonon coupling in magic-angle twisted bilayer graphene,” (2023), [arXiv:2303.14903](https://arxiv.org/abs/2303.14903) [[cond-mat.mes-hall](https://arxiv.org/archive/cond-mat)].
- [25] K. P. Nuckolls, R. L. Lee, M. Oh, D. Wong, T. Soejima, J. P. Hong, D. Călugăru, J. Herzog-Arbeitman, B. A. Bernevig, K. Watanabe, T. Taniguchi, N. Regnault, M. P. Zaletel, and A. Yazdani, “Quantum textures of the many-body wavefunctions in magic-angle graphene,” *Nature* **620**, 525 (2023).
- [26] Z. Zhou, J. Jiang, P. Karnatak, Z. Wang, G. Wagner, K. Watanabe, T. Taniguchi, C. Schönberger, S. A. Parameswaran, S. H. Simon, and M. Banerjee, “Double-dome Unconventional Superconductivity in Twisted Trilayer Graphene,” *arXiv e-prints* (2024), [arXiv:2404.09909](https://arxiv.org/abs/2404.09909) [[cond-mat.mes-hall](https://arxiv.org/archive/cond-mat)].
- [27] E. Lake, A. S. Patri, and T. Senthil, “Pairing symmetry of twisted bilayer graphene: A phenomenological synthesis,” *Phys. Rev. B* **106**, 104506 (2022).
- [28] H. D. Scammell, J. I. A. Li, and M. S. Scheurer, “Theory of zero-field superconducting diode effect in twisted trilayer graphene,” *2D Materials* **9**, 025027 (2022).
- [29] P. O. Sukhachov, F. von Oppen, and L. I. Glazman, “Andreev reflection in scanning tunneling spectroscopy of unconventional superconductors,” *Phys. Rev. Lett.* **130**, 216002 (2023).
- [30] C. Lewandowski, E. Lantagne-Hurtubise, A. Thomson, S. Nadj-Perge, and J. Alicea, “Andreev reflection spectroscopy in strongly paired superconductors,” *Phys. Rev. B* **107**, L020502 (2023).
- [31] H. Sainz-Cruz, P. A. Pantaleón, V. o. T. Phong, A. Jimeno-Pozo, and F. Guinea, “Junctions and superconducting symmetry in twisted bilayer graphene,” *Phys. Rev. Lett.* **131**, 016003 (2023).
- [32] M. Christos, S. Sachdev, and M. S. Scheurer, “Nodal band-off-diagonal superconductivity in twisted graphene superlattices,” *Nature Communications* **14**, 7134 (2023).
- [33] C.-X. Liu, Y. Chen, A. Yazdani, and B. A. Bernevig, “Electron-K-Phonon Interaction In Twisted Bilayer Graphene,” *arXiv e-prints* (2023), [arXiv:2303.15551](https://arxiv.org/abs/2303.15551) [[cond-mat.supr-con](https://arxiv.org/archive/cond-mat)].
- [34] P. P. Poduval and M. S. Scheurer, “Vestigial singlet pairing in a fluctuating magnetic triplet superconductor and its implications for graphene superlattices,” *Nature Communications* **15**, 1713 (2024).
- [35] L. Wang, E.-M. Shih, A. Ghiotto, L. Xian, D. A. Rhodes, C. Tan, M. Claassen, D. M. Kennes, Y. Bai, B. Kim, K. Watanabe, T. Taniguchi, X. Zhu, J. Hone, A. Rubio, A. N. Pasupathy, and C. R. Dean, “Correlated electronic phases in twisted bilayer transition metal dichalcogenides,” *Nature Materials* **19**, 861 (2020).
- [36] A. Ghiotto, E.-M. Shih, G. S. S. G. Pereira, D. A. Rhodes, B. Kim, J. Zang, A. J. Millis, K. Watanabe, T. Taniguchi, J. C. Hone, L. Wang, C. R. Dean, and A. N. Pasupathy, “Quantum criticality in twisted transition metal dichalcogenides,” *Nature* **597**, 345 (2021).
- [37] P. Knüppel, J. Zhu, Y. Xia, Z. Xia, Z. Han, Y. Zeng, K. Watanabe, T. Taniguchi, J. Shan, and K. F. Mak, “Correlated states controlled by tunable van Hove singularity in moiré WSe₂,” *arXiv e-prints* (2024), [arXiv:2406.03315](https://arxiv.org/abs/2406.03315) [[cond-mat.str-el](https://arxiv.org/archive/cond-mat)].
- [38] Y. Xia, Z. Han, K. Watanabe, T. Taniguchi, J. Shan, and K. F. Mak, “Unconventional superconductivity in twisted bilayer WSe₂,” *arXiv e-prints* (2024), [arXiv:2405.14784](https://arxiv.org/abs/2405.14784) [[cond-mat.mes-hall](https://arxiv.org/archive/cond-mat)].
- [39] Y. Guo, J. Pack, J. Swann, L. Holtzman, M. Cothrine, K. Watanabe, T. Taniguchi, D. Mandrus, K. Barmak, J. Hone, A. J. Millis, A. N. Pasupathy, and C. R. Dean, “Superconductivity in twisted bilayer WSe₂,” *arXiv e-prints* (2024), [arXiv:2406.03418](https://arxiv.org/abs/2406.03418) [[cond-mat.mes-hall](https://arxiv.org/archive/cond-mat)].
- [40] C. Schrade and L. Fu, “Nematic, chiral and topological superconductivity in transition metal dichalcogenides,” *arXiv e-prints* (2021), [arXiv:2110.10172](https://arxiv.org/abs/2110.10172) [[cond-mat.supr-con](https://arxiv.org/archive/cond-mat)].
- [41] T. Devakul, V. Crépel, Y. Zhang, and L. Fu, “Magic in twisted transition metal dichalcogenide bilayers,” *Nature Communications* **12**, 6730 (2021).
- [42] H. Pan, F. Wu, and S. Das Sarma, “Band topology, hubbard model, heisenberg model, and dzyaloshinskii-moriya interaction in twisted bilayer wse₂,” *Phys. Rev. Res.* **2**, 033087 (2020).
- [43] A. Wietek, J. Wang, J. Zang, J. Cano, A. Georges, and A. Millis, “Tunable stripe order and weak superconductivity in the moiré hubbard model,” *Phys. Rev. Res.* **4**, 043048 (2022).
- [44] J. Zang, J. Wang, J. Cano, and A. J. Millis, “Hartree-

- fock study of the moiré hubbard model for twisted bilayer transition metal dichalcogenides,” *Phys. Rev. B* **104**, 075150 (2021).
- [45] D. Kiese, Y. He, C. Hickey, A. Rubio, and D. M. Kennes, “TMDs as a platform for spin liquid physics: A strong coupling study of twisted bilayer WSe₂,” *APL Materials* **10**, 031113 (2022).
- [46] L. Klebl, A. Fischer, L. Classen, M. M. Scherer, and D. M. Kennes, “Competition of density waves and superconductivity in twisted tungsten diselenide,” *Phys. Rev. Res.* **5**, L012034 (2023).
- [47] J. Venderley and E.-A. Kim, “Density matrix renormalization group study of superconductivity in the triangular lattice hubbard model,” *Phys. Rev. B* **100**, 060506 (2019).
- [48] M. Bélanger, J. Fournier, and D. Sénéchal, “Superconductivity in the twisted bilayer transition metal dichalcogenide wse₂: A quantum cluster study,” *Phys. Rev. B* **106**, 235135 (2022).
- [49] F. Chen and D. N. Sheng, “Singlet, triplet, and pair density wave superconductivity in the doped triangular-lattice moiré system,” *Phys. Rev. B* **108**, L201110 (2023).
- [50] B. Zhou and Y.-H. Zhang, “Chiral and nodal superconductors in the t - j model with valley contrasting flux on a triangular moiré lattice,” *Phys. Rev. B* **108**, 155111 (2023).
- [51] M. Zegrodnik and A. Biborski, “Mixed singlet-triplet superconducting state within the moiré t - j - u model applied to twisted bilayer wse₂,” *Phys. Rev. B* **108**, 064506 (2023).
- [52] Y.-M. Wu, Z. Wu, and H. Yao, “Pair-density-wave and chiral superconductivity in twisted bilayer transition metal dichalcogenides,” *Phys. Rev. Lett.* **130**, 126001 (2023).
- [53] W. Akbar, A. Biborski, L. Rademaker, and M. Zegrodnik, “Topological superconductivity with mixed singlet-triplet pairing in moiré transition-metal-dichalcogenide bilayers,” arXiv e-prints (2024), [arXiv:2403.05903](https://arxiv.org/abs/2403.05903) [cond-mat.supr-con].
- [54] F. Wu, T. Lovorn, E. Tutuc, I. Martin, and A. H. MacDonald, “Topological insulators in twisted transition metal dichalcogenide homobilayers,” *Phys. Rev. Lett.* **122**, 086402 (2019).
- [55] Y.-T. Hsu, F. Wu, and S. Das Sarma, “Spin-valley locked instabilities in moiré transition metal dichalcogenides with conventional and higher-order van hove singularities,” *Phys. Rev. B* **104**, 195134 (2021).
- [56] S. Kim, J. F. Mendez-Valderrama, X. Wang, and D. Chowdhury, “Theory of Correlated Insulator(s) and Superconductor at $\nu = 1$ in Twisted WSe₂,” arXiv e-prints (2024), [arXiv:2406.03525](https://arxiv.org/abs/2406.03525) [cond-mat.str-el].
- [57] Since SU(2) spin rotation invariance is broken, one could also choose $\Theta = \eta_x \mathcal{K}$, cf. SI of Ref. 32; most notably, this would effectively swap A_1 and A_2 in Table II.
- [58] B. A. Bernevig, Z.-D. Song, N. Regnault, and B. Lian, “Twisted bilayer graphene. i. matrix elements, approximations, perturbation theory, and a $k \cdot p$ two-band model,” *Phys. Rev. B* **103**, 205411 (2021).
- [59] See Appendix for more information.
- [60] A. Thomson, S. Chatterjee, S. Sachdev, and M. S. Scheurer, “Triangular antiferromagnetism on the honeycomb lattice of twisted bilayer graphene,” *Phys. Rev. B* **98**, 075109 (2018).
- [61] T. Jolicoeur and J. C. Le Guillou, “Spin-wave results for the triangular heisenberg antiferromagnet,” *Phys. Rev. B* **40**, 2727 (1989).
- [62] B. Bernu, C. Lhuillier, and L. Pierre, “Signature of néel order in exact spectra of quantum antiferromagnets on finite lattices,” *Phys. Rev. Lett.* **69**, 2590 (1992).
- [63] R. Deutscher and H. U. Everts, “Thes=1/2 heisenberg antiferromagnet on the triangular lattice: Exact results and spin-wave theory for finite cells,” *Zeitschrift für Physik B Condensed Matter* **93**, 77 (1993).
- [64] A. V. C. Ar. Abanov and J. Schmalian, “Quantum-critical theory of the spin-fermion model and its application to cuprates: Normal state analysis,” *Advances in Physics* **52**, 119 (2003), <https://doi.org/10.1080/0001873021000057123>.
- [65] T. Sohler, E. Ponomarev, M. Gibertini, H. Berger, N. Marzari, N. Ubrig, and A. F. Morpurgo, “Enhanced electron-phonon interaction in multivalley materials,” *Phys. Rev. X* **9**, 031019 (2019).
- [66] A. Molina-Sánchez and L. Wirtz, “Phonons in single-layer and few-layer mos₂ and ws₂,” *Phys. Rev. B* **84**, 155413 (2011).
- [67] E. del Corro, A. Botello-Méndez, Y. Gillet, A. L. Elias, H. Terrones, S. Feng, C. Fantini, D. Rhodes, N. Pradhan, L. Balicas, X. Gonze, J. C. Charlier, M. Terrones, and M. A. Pimenta, “Atypical exciton-phonon interactions in ws₂ and wse₂ monolayers revealed by resonance raman spectroscopy,” *Nano Letters* **16**, 2363 (2016).
- [68] Z. Bi, N. F. Q. Yuan, and L. Fu, “Designing flat bands by strain,” *Phys. Rev. B* **100**, 035448 (2019).
- [69] J.-X. Hu, C.-P. Zhang, Y.-M. Xie, and K. T. Law, “Non-linear hall effects in strained twisted bilayer wse₂,” *Communications Physics* **5**, 255 (2022).
- [70] M. M. Scherer, D. M. Kennes, and L. Classen, “Chiral superconductivity with enhanced quantized hall responses in moirétransition metal dichalcogenides,” *npj Quantum Materials* **7**, 100 (2022).
- [71] K. Slagle and L. Fu, “Charge transfer excitations, pair density waves, and superconductivity in moiré materials,” *Phys. Rev. B* **102**, 235423 (2020).
- [72] V. Crépel, D. Guerci, J. Cano, J. H. Pixley, and A. Millis, “Topological superconductivity in doped magnetic moiré semiconductors,” *Phys. Rev. Lett.* **131**, 056001 (2023).
- [73] H. Wang, V. Harbola, Y.-J. Wu, P. A. van Aken, and J. Mannhart, “Interface Design Beyond Epitaxy: Oxide Heterostructures Comprising Symmetry-forbidden Interfaces,” arXiv e-prints (2024), [arXiv:2403.08736](https://arxiv.org/abs/2403.08736) [cond-mat.mtrl-sci].
- [74] B. Putzer, L. V. Pupim, and M. S. Scheurer, “Band theory for heterostructures with interface superlattices,” arXiv e-prints (2024), [arXiv:2404.12420](https://arxiv.org/abs/2404.12420) [cond-mat.mes-hall].
- [75] J. Zhu, Y.-Z. Chou, M. Xie, and S. Das Sarma, “Theory of superconductivity in twisted transition metal dichalcogenide homobilayers,” arXiv e-prints (2024), [arXiv:2406.19348](https://arxiv.org/abs/2406.19348) [cond-mat.supr-con].

Appendix A: Numerical solution of gap equation

The most general form of interactions in the space of the active bands we study for pairing is:

$$H_{\text{att.}} = -\frac{1}{A} \sum_{\mathbf{k}, \mathbf{k}'} \sum_{\mathbf{q}} \chi_{\mathbf{q}} d_{\mathbf{k}, \eta}^{\dagger} \lambda_j^{\eta \eta'}(\mathbf{k}, \mathbf{q}) d_{\mathbf{k}+\mathbf{q}, \eta'} d_{\mathbf{k}', \eta''}^{\dagger} \lambda_j^{\eta'' \eta'''}(\mathbf{k}', -\mathbf{q}) d_{\mathbf{k}'-\mathbf{q}, \eta'''} \quad (\text{A1})$$

where A is the sample area, \mathbf{k} and \mathbf{k}' are summed over the first Brillouin zone and \mathbf{q} is summed over all momenta. For intervalley fluctuations, i.e., fluctuations of $\phi_{x,y}$, we only keep $j = x, y$ in Eq. (A1); after using time-reversal symmetry to fix the gauge of the wavefunctions, we find the following LGE:

$$\left(\Delta_{\mathbf{k}}^{\dagger}\right)^{+-} = \sum_{\mathbf{q}} (\chi_{\mathbf{q}} + \chi_{-\mathbf{q}}) \frac{1 - 2n_F(E_{\mathbf{k}+\mathbf{q}}^+)}{2E_{\mathbf{k}+\mathbf{q}}^+} \left(\Delta_{\mathbf{k}+\mathbf{q}}^{\dagger}\right)^{-+} |\lambda_{x,y}^{+-}(\mathbf{k} + \mathbf{q}, -\mathbf{q})|^2 \quad (\text{A2})$$

Here $E_{\mathbf{k}+\mathbf{q}}^+$ is the dispersion in the + spin-valley flavor with the chemical potential fixed for every value of displacement field D such that hole-doping $\nu = 1$. $\Delta_{\mathbf{k}}^{\dagger}$ is defined as:

$$\left(\Delta_{\mathbf{k}}\right)^{\eta-\eta'} = \sum_{\mathbf{q}} (\chi_{\mathbf{q}} + \chi_{-\mathbf{q}}) \lambda_j^{\eta \eta'}(\mathbf{k}, \mathbf{q}) \langle d_{-\mathbf{k}-\mathbf{q}, -\eta'} d_{\mathbf{k}+\mathbf{q}, \eta'} \rangle \lambda_j^{-\eta-\eta'}(-\mathbf{k}, -\mathbf{q}) \quad (\text{A3})$$

In the case where there is more than one type of fluctuation contributing to pairing, the λ_j may be summed over $j = x, y, z, 0$ in the above. We also multiply the IVC interactions by an additional factor of $\frac{1}{2}$ relative to when we consider fluctuations of an order with only a single component, since at the level of the gap equation, λ_x and λ_y provide an identical contribution. After using Fermi-Dirac statistics, Eq. (A2) can be rewritten as:

$$\left(\Delta_{-\mathbf{k}}^{\dagger}\right)^{-+} = -\sum_{\mathbf{q}} (\chi_{\mathbf{q}} + \chi_{-\mathbf{q}}) \frac{1 - 2n_F(E_{\mathbf{k}+\mathbf{q}}^+)}{2E_{\mathbf{k}+\mathbf{q}}^+} \left(\Delta_{\mathbf{k}+\mathbf{q}}^{\dagger}\right)^{-+} |\lambda_{x,y}^{+-}(\mathbf{k} + \mathbf{q}, -\mathbf{q})|^2 \quad (\text{A4})$$

For VP fluctuations (ϕ_z) and, thus, $j = z$ in Eq. (A1), the LGE we solve is:

$$\left(\Delta_{\mathbf{k}}^{\dagger}\right)^{-+} = -\sum_{\mathbf{q}} (\chi_{\mathbf{q}} + \chi_{-\mathbf{q}}) \frac{1 - 2n_F(E_{\mathbf{k}+\mathbf{q}}^+)}{2E_{\mathbf{k}+\mathbf{q}}^+} \left(\Delta_{\mathbf{k}+\mathbf{q}}^{\dagger}\right)^{-+} |\lambda_z^{++}(\mathbf{k} + \mathbf{q}, -\mathbf{q})|^2 \quad (\text{A5})$$

The linearized gap equation for ϕ_0 , or equivalently the electron-phonon interactions we study, is the same as for VP fluctuations but with the opposite sign:

$$\left(\Delta_{\mathbf{k}}^{\dagger}\right)^{-+} = \sum_{\mathbf{q}} (\chi_{\mathbf{q}} + \chi_{-\mathbf{q}}) \frac{1 - 2n_F(E_{\mathbf{k}+\mathbf{q}}^+)}{2E_{\mathbf{k}+\mathbf{q}}^+} \left(\Delta_{\mathbf{k}+\mathbf{q}}^{\dagger}\right)^{-+} |\lambda_0^{++}(\mathbf{k} + \mathbf{q}, -\mathbf{q})|^2 \quad (\text{A6})$$

Unless otherwise specified, all solutions are calculated at $T = 1$ K. We sum \mathbf{q} out to 2 shells outside the first Brillouin zone, an approximation justified by the falling off of both the form factors and $\chi_{\mathbf{q}}$.

For the case where we study the relative strength of different types of fluctuations or phonons (ϕ_0), for example, IVC fluctuations ($\phi_{x,y}$) and phonons [in Fig. 3(a-d) of the main text], we solve a gap equation of the following form:

$$\begin{aligned} \left(\Delta_{\mathbf{k}}^{\dagger}\right)^{-+} = & -(1-x) \sum_{\mathbf{q}} (\chi_{\mathbf{q}} + \chi_{-\mathbf{q}}) \frac{1 - 2n_F(E_{-\mathbf{k}-\mathbf{q}}^+)}{2E_{-\mathbf{k}-\mathbf{q}}^+} \left(\Delta_{-\mathbf{k}-\mathbf{q}}^{\dagger}\right)^{-+} |\lambda_{x,y}^{+-}(-\mathbf{k} - \mathbf{q}, \mathbf{q})|^2 \\ & + x \sum_{\mathbf{q}} (\chi_{\mathbf{q}} + \chi_{-\mathbf{q}}) \frac{1 - 2n_F(E_{\mathbf{k}+\mathbf{q}}^+)}{2E_{\mathbf{k}+\mathbf{q}}^+} \left(\Delta_{\mathbf{k}+\mathbf{q}}^{\dagger}\right)^{-+} |\lambda_0^{++}(\mathbf{k} + \mathbf{q}, -\mathbf{q})|^2 \end{aligned} \quad (\text{A7})$$

where x is a parameter which is used to tune the relative strengths of each interactions.

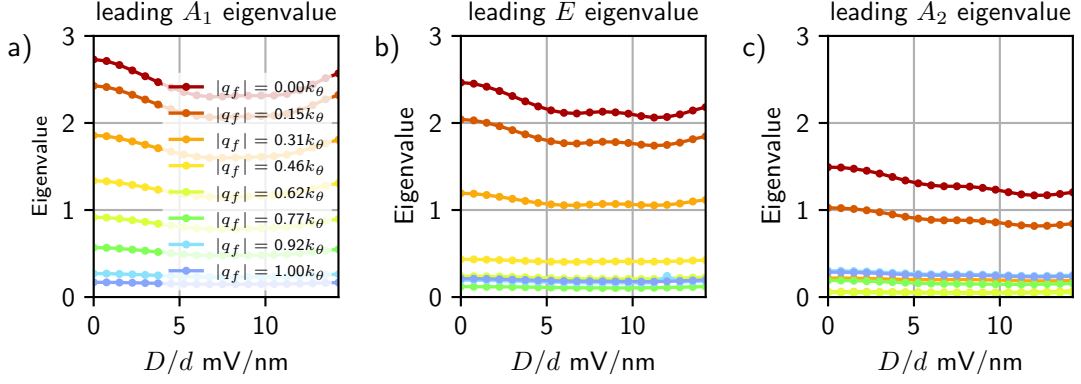


FIG. 4: We plot the leading eigenvalues corresponding to the A_1 (a), E (b), and A_2 (c) representations for varying wave-vectors \mathbf{q}_f at with IVC fluctuations ($\phi_{x,y}$). We use a gap parameter $\alpha = 0.25$ in $\chi(\mathbf{q})$.

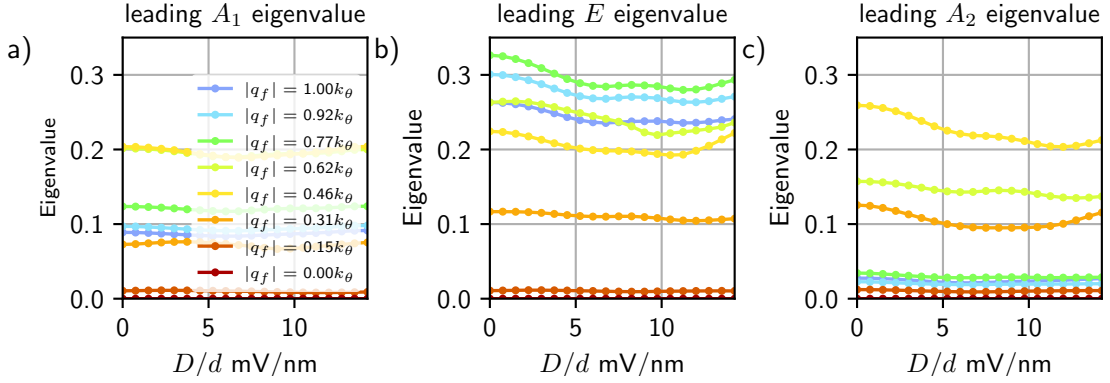


FIG. 5: We plot the leading eigenvalues corresponding to the A_1 (a), E (b), and A_2 (c) representations for varying wave-vectors \mathbf{q}_f with VP fluctuations (ϕ_z). We use a gap parameter $\alpha = 0.25$ in $\chi(\mathbf{q})$. We note the eigenvalues here are significantly smaller than for the case of IVC fluctuations with the same coupling strength and the relative dominance of the E state.

Appendix B: Additional numerical results

In this supplement, we present solutions of the LGE in the presence of additional perturbations, interactions, or potentials not explicitly shown in the main text. In Fig. 4, we show the leading eigenvalues for each IR for a potential $\chi(\mathbf{q}) = \frac{C\alpha}{\alpha^2 + (\mathbf{q} - \mathbf{q}_f)^2/k_\theta^2} + \frac{C\alpha}{\alpha^2 + (\mathbf{q} - C_{3z}\mathbf{q}_f)^2/k_\theta^2} + \frac{C\alpha}{\alpha^2 + (\mathbf{q} - C_{3z}^2\mathbf{q}_f)^2/k_\theta^2}$ with gap parameter $\alpha = 0.25$ for different values of \mathbf{q}_f and IVC fluctuations. We choose \mathbf{q}_f to lie along the contour between the Γ point and \mathbf{K} point in the moiré Brillouin zone. We also present the same type of plots for VP fluctuations in Fig. 5. Furthermore, we illustrate the impact of competition between $\phi_{x,y}$ and ϕ_z fluctuations in Fig. 6, where as in the case of phonons, we parameterize their relative strengths with a dimensionless parameter, now g instead of x , and normalize the contribution from the two component $\phi_{x,y}$ fluctuations by a factor of 2. One can see that VP fluctuations are detrimental to pairing. In Fig. 7, we study the LGE for layer-odd IVC ($\phi_{x,y}$) fluctuations and demonstrate that our conclusions do not strongly depend on whether the fluctuations are layer even or odd. What is more, we check the flat metric condition both with and without a nonzero displacement field in Fig. 8. Apart from a peak close to Γ , the form factors are approximately independent of \mathbf{k} for $\mathbf{q} = \mathbf{G} \in \text{RL}$. Finally, we show the leading basis functions, which are more sharply peaked around the Fermi surface, for $D/d = 14.45$ mV/nm and $\alpha = 0.1$ in Fig. 9 to demonstrate how a smaller α affects the solutions we find.

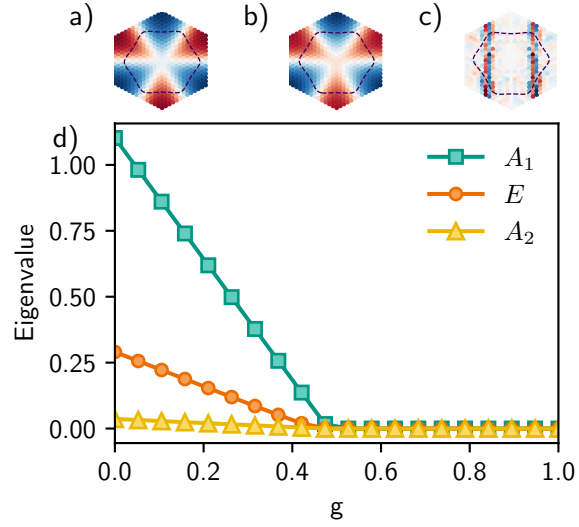


FIG. 6: We fix $D/d = 14.45$ mV/nm and plot the leading eigenvalue corresponding to relative couplings g between IVC fluctuations and VP fluctuations for $g = 0$ (a), and $g = 0.42$ (b), and $g = 1$ (c), as well as the leading eigenvalues for the A_1 , A_2 , and E representations as a function of g .

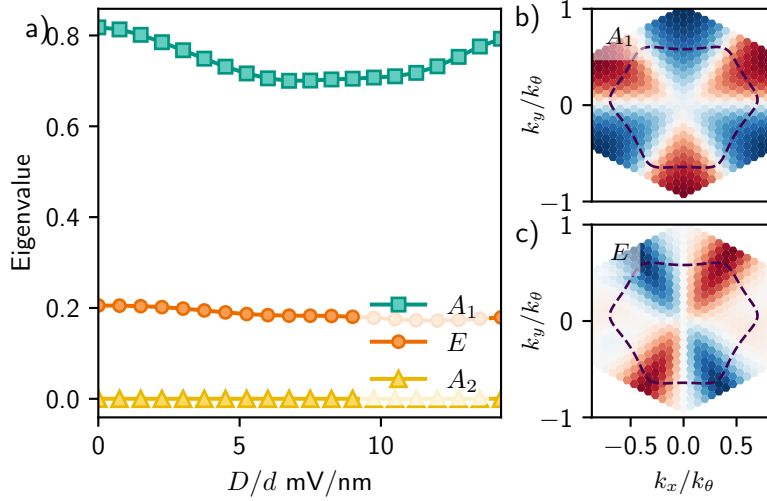


FIG. 7: We plot eigenvalue as a function of displacement field (a) as well as the leading (b) and subleading (c) basis functions as a function of displacement field for layer-odd fluctuations of $\phi_{x,y}$.

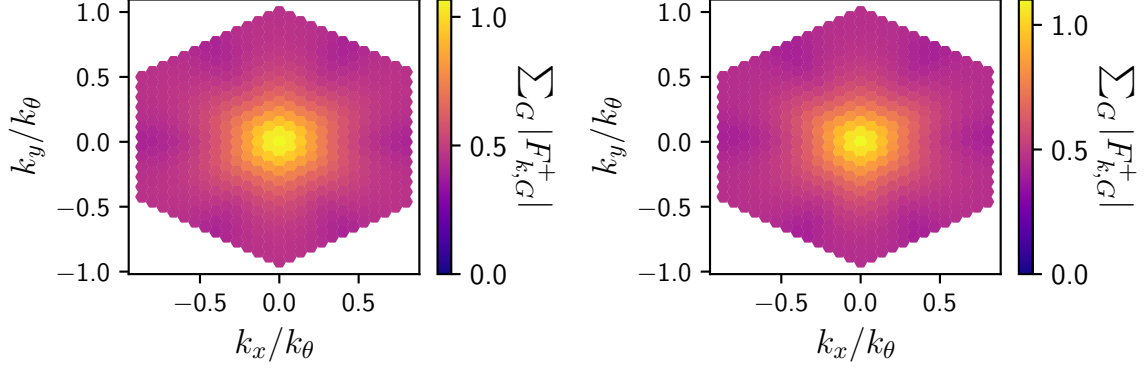


FIG. 8: We plot $\sum_G |F_{k,G}^+|$ for the six smallest nonzero \mathbf{G} reciprocal lattice vectors for $D/d = 0$ and $D/d = 14.45$ mV/nm.

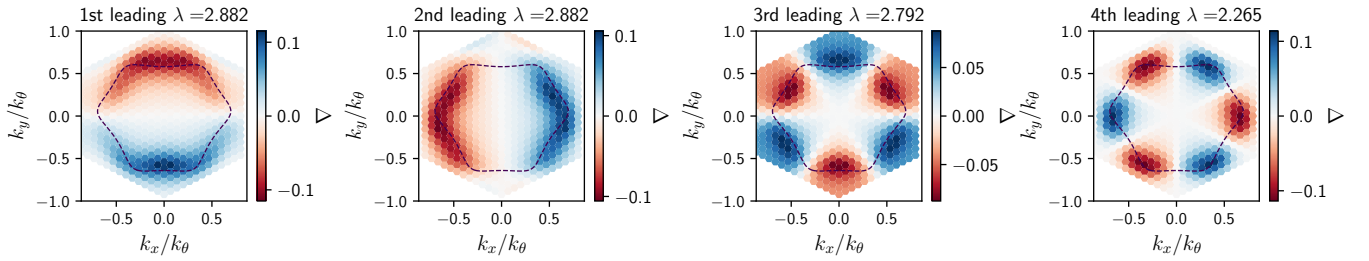


FIG. 9: Basis functions at $D/d = 14.45$ mV/nm with $\alpha = 0.1$ for fluctuations of $\phi_{x,y}$.